scientific reports

OPEN

A comparative study of advanced evolutionary algorithms for optimizing microgrid performance under dynamic pricing conditions

Rasha Elazab, Ahmed T. Abdelnaby✉ & A.A. Ali

The integration of microgrids into the existing power system framework enhances the reliability and efficiency of the utility grid. This manuscript presents an innovative mathematical paradigm designed for the optimization of both the structural and operational aspects of a grid-connected microgrid, leveraging the principles of Demand-Side Management (DSM). The focus of this work lies in a comprehensive exploration of the implications brought about by the Renewable Generation-Based Dynamic Pricing Demand Response (RGDP-DR) mechanism, particularly in terms of its influence on the optimal microgrid configuration, considering perspectives from end-users and the utility entity. This inquiry is rooted in a holistic assessment that encompasses technical and economic performance benchmarks. The RGDP-induced DR framework adeptly addresses the needs of the consumer base, showcasing notable efficiency and economic feasibility. To address the intricate nonlinear optimization challenge at hand, we employ an evolutionary algorithm named the "Dandelion Algorithm" (DA). A rigorous comparative study is conducted to evaluate the efficacy of four optimization techniques, affirming the supremacy of the proposed DA. Within this discourse, the complexity of microgrid sizing is cast as a dual-objective optimization task. The twin objectives involve minimizing the aggregate annual outlay and reducing emissions. The results of this endeavor unequivocally endorse the superiority of the DA over its counterparts. The DA demonstrates exceptional proficiency in orchestrating the most cost-effective microgrid and consumer invoice, surpassing the performance of alternative optimization methodologies.

List of symbols

N_S	The number of PV modules
F_S	PV reduction factor
$P_L^Z(t)$	zth Scenario load power (kW)
$\rho_o(i)$	The initial electricity price ($)
$P_L(i)$	The initial load demand (kW)
$E(i,i)$	Self-elasticity
$E(i,j)$	Cross-elasticity
$\rho_{rgdp}(i)$	The RGDP electricity price ($/kWh).
$P_L^{RGDP}(i)$	The final economic RGDP load model (kWh)
e_i	The orbital eccentricity for the i th planet.
$R_i(t)$	The Euclidian distance
$V_i(t)$	The i th planet velocity.
φ	A random number between zero and one.
λ	A number produced based on levy flight.
ξ	An indicator to reorient the search.
h	A variable used to regulate how far the Sun is from the planet i.
$SOC(t)$	Battery state of charge (kWh)

Faculty of Engineering, Helwan University, Cairo, Egypt. ✉email: ahmed.tarek1@h-eng.helwan.edu.eg

E_{pen}	Emissions penalty (\$/ton)
RPC_{AN}	Annual replacement cost
OMC_{AN}	Annual operating and maintenance cost
D_r	Real discount rate (%)
N_k	kth Component number of units
P_{R_k}	kth Component rated capacity (kW)
C_{i_k}	kth Component initial cost (\$/kW)
NR_k	kth Component number of replacements
L_k	kth Component lifetime (years)
F_k	kth Component emissions (kgCO$_2$-eq/kWh)
E_k	kth Component produced energy (kWh)
X_{elite}	The dandelion seed's best position
T_i	The i th planet orbital period
$F_{g_i}(t)$	The attraction force
μ	A number produced using random numbers ranging from 0 to 1, levy-flight, and normal distribution.
l	A linearly decreasing factor from 1.0 to 0.0.
δ	The likelihood of nutcrackers travelling across the entire search space to look for unreachable locations

In contemporary energy landscapes, there has been a noteworthy upswing in the integration of Renewable Energy Sources (RES) with the grid, driven by a commitment to reduce greenhouse gas emissions from conventional fossil fuel-based power plants[1]. This transformative era has witnessed the ascendancy of decentralized RES, strategically positioned to optimize clean energy generation across extensive geographical domains, culminating in the emergence of Microgrid (MG) concepts as compact-scale networks[2].

Energizing the paradigm of Demand-Side Management (DSM), this paper underscores the imperative for customers to manipulate their energy consumption patterns. The effective application of DSM brings multifaceted benefits, including enhanced system reliability, improved efficiency, reduced microgrid operational costs, optimized load patterns, minimized power outages, decreased carbon emissions, and increased customer satisfaction. Within Demand Response (DR), specifically, load modification strategies, a subset of DSM, various tactics such as strategic load growth, load shifting, valley filling, peak clipping, strategic conservation, and flexible load shaping are employed[3]. These strategies fall into two main approaches: incentive-based and price-based paradigms[4]. The former encompasses initiatives such as demand buyback/bidding schemes[5], curtailable / interruptible services[6], ancillary service programs[7], emergency DR programs[8], capacity market programs[9], and direct load control mechanisms[10]. Conversely, the latter embraces strategies: Time-of-Use (TOU), fixed pricing, real-time pricing, and critical peak pricing models[11].

In the microgrid planning scope, two pivotal factors—the operator perspective and the client outlook—significantly influence the effectiveness of DSM deployment. From the client's standpoint, electricity bill expenditure is ameliorated, while on the operator's side, DSM engenders a reduction in microgrid overheads and mitigates risks entailed by power deficits[12]. The literature summarizes an array of techniques and mathematical formulations underpinning DSM within MG applications[13], with a notable exploration into the comparative assessment of diverse Energy Storage Systems (ESS) for DSM through industrial installations detailed in[14].

However, the intricate challenge of microgrid sizing, entangled with non-linear constraints, necessitates the integration of DR programs. Recent initiatives explored in references[15–17] investigated Incentive-Based Demand Response Programs (IDRPs) employing the Sparrow Algorithm, Black Widow Algorithm (BWA), and Whale Algorithm to reduce operational expenses. The practice of load shifting was examined using Mixed-Integer Linear Programming (MILP), Genetic Algorithm (GA), and Augmented ε-Constraint techniques to optimize overall expenditures[18–20]. TOU strategies are featured with BWA, GA, hybrid optimization multi-energy resource, and pseudo-gravitational algorithm to drive cost reduction[21–24].

In[25–28], the optimal sizing of various microgrids considering energy management techniques using several optimization algorithms has been discussed.

In 2020, Renewable Generation-Based Dynamic Pricing (RGDP) DR was proposed in[29] to minimize the total MG cost of an isolated microgrid using MILP. RGDP-DR achieves a zero reduction in energy consumption and maximum customer satisfaction. However, this paper adopts RGDP DR to minimize life cycle emissions and the overall cost of grid-tied MG using the Dandelion Algorithm (DA).

Given the aforementioned investigations, the commonality across prior studies is the trade-off between DR-driven energy reduction and customer satisfaction. This research addresses this gap by introducing a novel DR strategy termed RGDP DR, designed for rescheduling load demands within grid-connected MGs while prioritizing customer satisfaction. To effectively handle this intricate challenge, a novel meta-heuristic approach called the Dandelion Algorithm (DA) is proposed. The primary objective of this algorithm is to determine optimal capacities for distributed energy sources within the microgrid, taking into account the complexities of DSM. A comprehensive comparative analysis is undertaken, comparing the performance of the DA against three alternative optimization methods within the context of grid-connected MGs influenced by the RGDP DR strategy. Through the utilization of MATLAB/M-files simulation software, a mathematical model of the grid-connected MG is established, incorporating the RGDP DR strategy and various optimization techniques. This model serves to demonstrate the effectiveness of the proposed approach in contrast to its counterparts.

Moreover, the modifications introduced in our study are crucial for the specific context of grid-connected microgrids. While the original mathematical model[29] was formulated for an isolated microgrid, we have diligently

adapted and validated the model to align with the distinctive characteristics of a grid-tied microgrid. This adaptation encompasses the inclusion of considerations for energy exchange with the utility grid—a facet not explicitly addressed in earlier literature focused on isolated microgrids. The cost functions have been appropriately modified to account for this interaction with the utility grid. More precisely, we have incorporated the price of energy exchanged with the utility grid into the cost functions. This refinement ensures a more precise representation of the economic dynamics and operational constraints inherent in grid-connected microgrids. By doing so, our study provides a comprehensive perspective on the optimization challenges and opportunities specifically applicable to the context of grid-connected microgrids.

The prime contributions of this study are concisely summarized as follows:

- Pioneering the integration of a groundbreaking price-based DR paradigm, namely RGDP DR, designed to ensure maximal customer contentment at a reduced operational outlay, within the context of grid-connected MGs.
- Developing an innovative mathematical framework that seamlessly integrates the Demand Response (DR) approach into the optimization challenge of identifying the most efficient dimensions for grid-connected microgrids. This framework aims to achieve two simultaneous goals: the reduction of overall costs and the mitigation of emissions.
- Introducing a cutting-edge metaheuristic algorithm, DA, specifically designed to adeptly address the complexities associated with optimizing the size of grid-connected microgrids. The algorithm capitalizes on technical and economic metrics to effectively navigate the inherent intricacies of this optimization problem.

The subsequent sections of the paper are systematically organized as follows: Section "Modeling and configuration of system components" provides a concise explanation of the configuration and modeling complexities related to the proposed grid-connected MG. Section "Problem formulation" presents the formulation of the optimization challenge, incorporating the system's inherent constraints. In Section "RGDP-DR program", a comprehensive depiction of the RGDP DR strategy is provided, along with its intricate modeling. The methodologies underlying the utilization of four distinct optimization techniques to address the optimization problem are concisely summarized in Section "Optimization techniques". Moving forward, Section "Results and discussion" serves as a platform for a thorough examination and discussion of the simulation outcomes across four distinct scenarios. Bringing the discussion to a close, Section "Conclusion" summarizes the cumulative conclusion of this study.

Modeling and configuration of system components

Figure 1 illustrates the arrangement of the proposed MG as described. This MG design incorporates a trio of RES: photovoltaic (PV) panels, battery storage units, and Wind Turbines (WTs). Additionally, a converter is incorporated into the setup to establish a connection between the AC and DC buses. On a specified day, MG registers a peak demand of 2115.4 kW, with a corresponding energy consumption of roughly 21,117.7 kWh. The detailed model for each RES will be discussed in the following subsections:

PV modeling

The PV-generated power $P_S(t)$ can be computed using Eq. (1) [30].

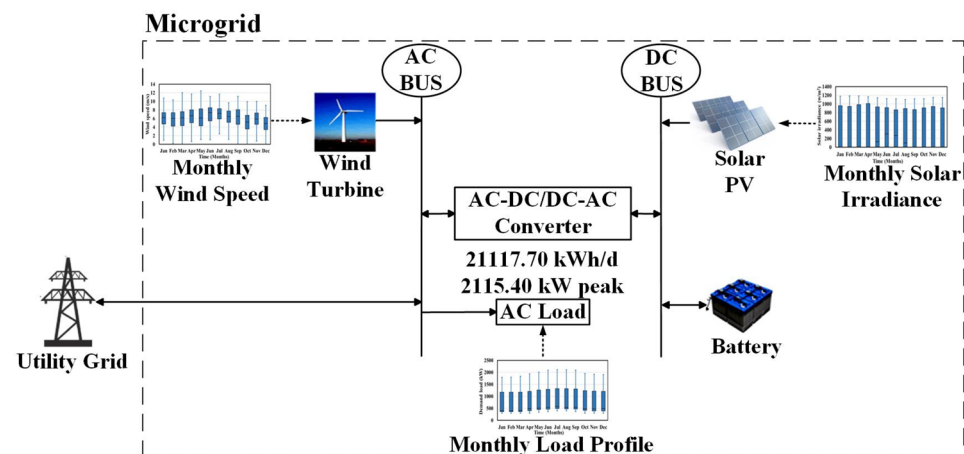$$P_S(t) = N_S \times P_{STC} \times F_S \times \frac{I(t)}{1000} \tag{1}$$

Figure 1. The studied grid-tied MG.

where N_S is the number of PV modules, P_{STC} is the PV power rating at STC (kW), F_S is the PV module reduction factor, and $I(t)$ is the global solar irradiance (W/m²).

WT modeling
WT output power $P_w(t)$ can be defined using Eq. (2)[31].

$$P_w(t) = \begin{cases} 0 & 0 \leq v(t) \leq v_{ci} \\ N_w \times P_r \times \frac{v^2(t) - v_{ci}^2}{v_r^2 - v_{ci}^2} & v_{ci} \leq v(t) \leq v_r \\ N_w \times P_r & v_r \leq v(t) \leq v_{co} \\ 0 & v(t) \geq v_{co} \end{cases} \tag{2}$$

where P_r is the WT's rated power, and N_w is the number of WTs.

Modeling of the battery energy storage system
Recently, the utilization of lithium-ion batteries has become prevalent in MG applications due to their remarkable characteristics, including high power density, significant energy density, and prolonged lifespan. Battery Energy Storage Systems (BESS) function through three distinct operational modes: charging, discharging, and idle mode.

Charging mode
In instances where the power generated by MG sources exceeds load requirements, the excess power is directed toward charging the battery. Consequently, the methodology outlined below is employed to calculate the accumulated energy from this charging process[32,33]:

$$P_{CH}(t) = \left(P_S(t) + \eta_{CON} \times (P_W(t) - P_L^Z(t)) \right) \times \eta_{CH} \tag{3}$$

where $P_{CH}(t)$ is the power being charged at time t, $P_L^Z(t)$ signifies the load power of the scenario indexed as the zth at time t, and subscript z indicates the specific scenarios under consideration. $E_{CH}(t)$ represents the energy being charged during the time interval Δt, which is typically an hour. The efficiencies of the converter and charging processes are denoted as η_{CON} and η_{CH}, respectively.

The battery State of Charge (*SOC*) is calculated as:

$$SOC(t) = SOC(t-1) + P_{CH}(t) \times \Delta t \tag{4}$$

where $SOC(t)$ and $SOC(t-1)$ are states of charge at two successive time instants of t and $t-1$, respectively.

When the calculated $P_{CH}(t)$ is greater than $(SOC_{max} - SOC(t-1))$, the power can be sold to the connected grid $P_{GS}(t)$ and calculated as:

$$P_{GS}(t) \times \Delta t = P_{CH}(t) \times \Delta t - SOC_{max} + SOC(t-1) \tag{5}$$

where SOC_{max} refers to the maximum SOC of the battery.

Discharging mode
In cases where the energy demand of a load exceeds the output power of PV and WTs, the battery is discharged. The subsequent energy discharged and the corresponding SOC can be approximated using the following approach[32,33]:

$$P_{DIS}(t) = \frac{\frac{P_L^Z(t) - P_W(t)}{\eta_{CON}} - P_S(t)}{\eta_{DIS}} \tag{6}$$

$$SOC(t) = SOC(t-1) - P_{DIS}(t) \times \Delta t \tag{7}$$

where $P_{DIS}(t)$ is battery discharging power at time t, $E_{DIS}(t)$ stands for discharging energy. η_{DIS} is the discharging efficiency.

In the event of a battery power shortage, the purchased grid power $P_{GP}(t)$ can be defined as:

$$P_{GP}(t) \times \Delta t = P_{DIS}(t) \times \Delta t - SOC(t-1) + SOC_{min} \tag{8}$$

where SOC_{min} is the battery minimum permissible SOC.

Ideal mode
Upon reaching full charge, the surplus MG-generated power can be sold back to the grid. This situation is depicted as follows[34]:

$$P_{GS}(t) = P_W(t) - P_L^Z(t) + P_S(t) \times \eta_{CON} \tag{9}$$

Once the battery's maximum discharge capacity is reached, any additional power needed will be procured from the grid. This scenario can be articulated as follows:

$$P_{GP}(t) = P_L^Z(t) - P_W(t) - P_S(t) \times \eta_{CON} \tag{10}$$

Problem formulation

This section outlines the technical constraints on the system as well as the optimization problem's objective functions.

The objective functions (OFs)

The study addresses the comprehensive OF inherent in the optimization challenge of microgrid (MG) sizing. The primary objective of this Objective Function (OF) is to simultaneously minimize the Total Annual Cost (TAC) as presented in Eq. (12) and reduce Life Cycle Emissions (LCE) as defined in Eq. (17) within the context of grid-interconnected MG. The optimization process considers operational constraints delineated in Eqs. (18) to (24). Consequently, the overarching objective function is composed of two metrics, each of which is characterized by a specific weight ratio. Therefore, the formulation of the OF is presented as follows:

$$\min_x(OF) = \min_x\left(\varphi_1 * TAC + \varphi_2 * \frac{E_{pen} * LCE}{1000}\right) \tag{11}$$

where x represents a vector containing optimization parameters: the power output of sources, storage, and converter. E_{pen} stands for the penalty associated with CO_2 emissions (\$/ton). The assigned values for φ_1 and φ_2 are both set to 0.5.

TAC minimization
It can be calculated as follows[29]:

$$TAC = CC_{AN} + RPC_{AN} + OMC_{AN} - SVC_{AN} \tag{12}$$

where CC_{AN}, RPC_{AN}, OMC_{AN}, and SVC_{AN} are MG annual capital costs of the MG components, replacement costs, operating and maintenance costs, and salvage costs, respectively.

<u>Components' capital costs.</u> The total yearly MG components' capital cost can be determined using Eq. (13)[35]:

$$CC_{AN} = \sum_{k=1}^{K}\left\{N_k \times P_{R\_k} \times C_{i\_k} * \frac{D_r(1+D_r)^T}{(1+D_r)^T - 1}\right\} \tag{13}$$

where N_k indicates the number of kth component units, P_{R_k} is the capacity in kW of kth component, C_{i_k} is the kth component initial cost in (\$/kW), K is the number of system components, D_r indicates the reduction rate (%), T is the project's lifetime, and k indicates the MG components, which are WT, BESS, PV, and converter.

<u>Replacement costs.</u> If the lifetimes of microgrid (MG) components are shorter than the lifespan of the project, they need to be replaced. The overall annual cost of replacing MG components can be calculated using Eq. (14)[36]:

$$RPC_{AN} = \sum_{k=1}^{K}\left\{N_k \times P_{R\_k} \times C_{r\_k} \times \sum_{m=1}^{NR_k}\left(\frac{1}{1+D_r}\right)^{(m \times L_k)}\right\} * \frac{D_r(1+D_r)^T}{(1+D_r)^T - 1} \tag{14}$$

where NR_k indicates the number of kth component replacements, L_k is the lifetime in years, and C_{r_k} is the cost of unit replacement (\$/kW).

<u>Operating and maintenance O&M costs.</u> Annual O&M costs can be described as[29,30]:

$$OMC_{AN} = \sum_{k=1}^{K}\left\{N_k * P_{R\_k} * C_{om\_k}\right\} + \sum_{t=1}^{8760}\left\{C_{gp}(t) * P_{gp}(t) - C_{gs}(t) * P_{gs}(t)\right\} \tag{15}$$

where C_{om_k} is the kth component annual O&M costs in \$/kW/Year, $C_{gp}(t)$ is the per-unit buying grid power cost at tth hour in \$/kW/Year, $P_{gp}(t)$ (kW) is the purchased power from the utility during the tth hour, $C_{gs}(t)$ is the price of the grid sold power in \$/kW/Year, and $P_{gs}(t)$ (kW) is the utility sold power.

<u>Salvage costs.</u> The annual MG components' salvage cost can be written as[37]:

$$SVC_{AN} = \sum_{k=1}^{K}\left\{N_k * P_{R\_k} * C_{r\_k} * \frac{L_k - (T - (L_k * NR_k))}{L_k} * \left(\frac{1}{1+D_r}\right)^T\right\} * \frac{D_r(1+D_r)^T}{(1+D_r)^T - 1} \tag{16}$$

Minimizing LCE
LCE In kilograms of CO_2-equivalent per year represents the cumulative carbon dioxide (CO_2) emissions from microgrid components over their complete lifecycle. This value can be computed using the formula outlined in reference[32]:

$$\text{LCE} = \sum_{k=1}^{K} F_k E_k \tag{17}$$

where F_k is the kth component annual CO_2 emissions in kgCO_2-eq/kWh and E_k is the annual generated energy in kWh. MG's detailed characteristics are presented[34].

Operational parameters of MG components must adhere to established limits to ensure the integrity and dependability of the power supply infrastructure.

The technical constraints

Operational parameters of MG components must adhere to established limits to ensure the integrity and dependability of the power supply infrastructure. Inequality and power balance constraints should be calculated and considered, as will be described in the following paragraphs.

The inequality constraints

Maximum and minimum boundaries of MG sources should be satisfied, as follows[34]:

$$0 \le P_S(t) \le P_{S\_max} \tag{18}$$

$$0 \le P_w(t) \le P_{w\_max} \tag{19}$$

$$-P_{CH\_max} \le P_b(t) \le P_{DIS\_max} \tag{20}$$

$$0 \le |P_{INV}(t)| \le P_{inv\_max} \tag{21}$$

where $P_b(t)$ is storage power. P_{S_max}, P_{w_max}, and P_{inv_max} are RESs and converter capacities, respectively. P_{CH_max} and P_{DIS_max} represent the maximum battery charging and maximum battery discharging, respectively.

The SOC of the battery must be maintained within the acceptable range, as deep discharges and overcharging can both lead to a reduction in battery lifespan, as explained below[32,33]:

$$SOC_{min} \le SOC(t) \le SOC_{max} \tag{22}$$

At time i, the RGDP electrical cost $\rho_{rgdp}(i)$ must be within the allowable limits as follows[29]:

$$\rho_{min} \le \rho_{rgdp}(i) \le \rho_{max} \tag{23}$$

where ρ_{min} and ρ_{max} are the minimum and maximum prices, respectively.

The power balance constraints

Power equilibrium can be achieved through the utilization of the subsequent expression[34]:

$$P_L^Z(t) = P_{GP}(t) - P_{GS}(t) + P_W(t) + \left(P_S(t) + P_{DIS}(t) \times \eta_{DIS} - \frac{P_{CH}(t)}{\eta_{CH}} \right) \times \eta_{CON} \tag{24}$$

RGDP-DR program

An energy management strategy that enables the modification of load patterns is known as DR, where electricity consumption is modified by shifting it from high-demand to low-demand periods or by reducing usage during peak periods. Conventional DR approaches often lead to reduced energy consumption, though they might impact customer satisfaction. On the contrary, the RGDP-DR program distinguishes itself by achieving optimal equilibrium. This program guarantees no reduction in energy consumption, thereby achieving the utmost customer satisfaction, as expounded in this section.

The self-elasticity coefficient $E(i,i)$ refers to the sensitivity of (i) hour demand to (i) hour price and can be expressed using Eq. (25) as follows[29]:

$$E(i,i) = \frac{\rho_o(i)}{P_L(i)} \times \frac{\partial P_L(i)}{\partial \rho(i)} \, i = 1, 2, \ldots, 24 \tag{25}$$

where $\rho_o(i)$ is the initial electrical cost, $P_L(i)$ is the initial demand, $\partial P_L(i)$ represents the demand variance during period i, and $\partial \rho(i)$ indicates the cost fluctuation during the i period.

The cross-elasticity coefficient $E(i,j)$ reflects the (i) demand sensitivity to (j) price and is calculated using Eq. (26) as follows[29]:

$$E(i,j) = \frac{\rho_o(j)}{P_L(i)} \times \frac{\partial P_L(i)}{\partial \rho(j)} \, i, j = 1, 2, \ldots, 24 \tag{26}$$

Table 1 shows the applied cross- and self-elasticities of the demand load in this research.

RGDP signifies an advanced evolution of time-based Demand Response (DR) programs. This advancement arises from the shift in the DR electricity price, moving from a variable independent of microgrid (MG) configuration to a dynamic value linked to the disparity between energy demand and the Renewable Energy Source

	Peak	Off-peak	Valley
Peak	− 0.100	0.0160	0.0120
Off-peak	0.0160	− 0.100	0.010
Valley	0.0120	0.010	− 0.100

Table 1. Cross and self-elasticity coefficients[38].

(RES) output. Furthermore, RGDP's primary objective is to mitigate customer dissatisfaction while simultaneously enhancing utility for the electricity provider.

Consequently, the price structure offered motivates participants to simply reschedule energy usage patterns. As specified in Eq. (27), the comprehensive energy consumption of a participant should remain comparatively consistent both before and after the RGDP DR program's implementation[29].

$$\sum_{i=1}^{24} P_L^{RGDP}(i) = \sum_{i=1}^{24} P_L(i) \tag{27}$$

The RGDP tariff is quantified as follows[29]:

$$\rho_{rgdp}(i) = \rho_0(i) \times \left\{ 1 + \frac{P_L(i) - P_W(i) - P_S(i) \times \eta_{CON}}{P_L(i)} \right\} \tag{28}$$

The RGDP economic load model is acquired by[29]:

$$P_L^{RGDP}(i) = P_L(i) \times \left\{ 1 + E(i,i) \times \frac{[\rho_{rgdp}(i) - \rho_0(i)]}{\rho_0(i)} + \sum_{\substack{j=1 \\ j \neq i}}^{24} E(i,j) \times \frac{[\rho_{rgdp}(j) - \rho_0(j)]}{\rho_0(j)} \right\} \tag{29}$$

Optimization techniques
Four optimization techniques applied in this paper are mathematically modelled in this section.

PSO algorithm
Eberhart and Kennedy first presented PSO[39]. This algorithm draws inspiration from the flocking behavior of birds aiming to reach a target, with each individual's actions influencing the group's collective movement. In PSO, particles symbolize potential solutions dispersed within the search space to address a given problem. The PSO methodology encompasses five fundamental stages:

- *Initialization* The initial setup of particles and their attributes.
- *Evaluation* The assessment of each particle's fitness based on the defined objective function.
- *Updating Particle Best (Pbest)* Individual particles update their personal best solution based on their current fitness.
- *Updating Global Best (Gbest)* The best solution among all particles is updated.
- *Updating Velocity and Location* Particles adjust their velocity and position, guided by both Pbest and Gbest, iteratively moving towards a globally optimal solution.

Particles in PSO emulate the trajectories set by Pbest and Gbest, dynamically altering their directions to progressively converge towards the problem's global optimal solution.

Kepler optimization algorithm (KOA)
KOA draws inspiration from Kepler's planetary motion laws, utilizing them for forecasting the planets' positions and velocities at any specific moment[40]. Within the KOA framework, individual planets, characterized by their respective positions, assume the role of candidate solutions. These planetary positions are iteratively adjusted during the optimization process, referencing the best solution achieved thus far (analogous to the Sun in the solar system). The operational steps of the KOA are visually depicted in the provided flow chart, Fig. 2, illustrating the algorithm's computational procedures and its systematic optimization approach.

According to Fig. 2, KOA can be summarized as follows:

Initialization process
The initial population of planets will be generated randomly within the defined boundaries of the search space, according to Eq. (30):
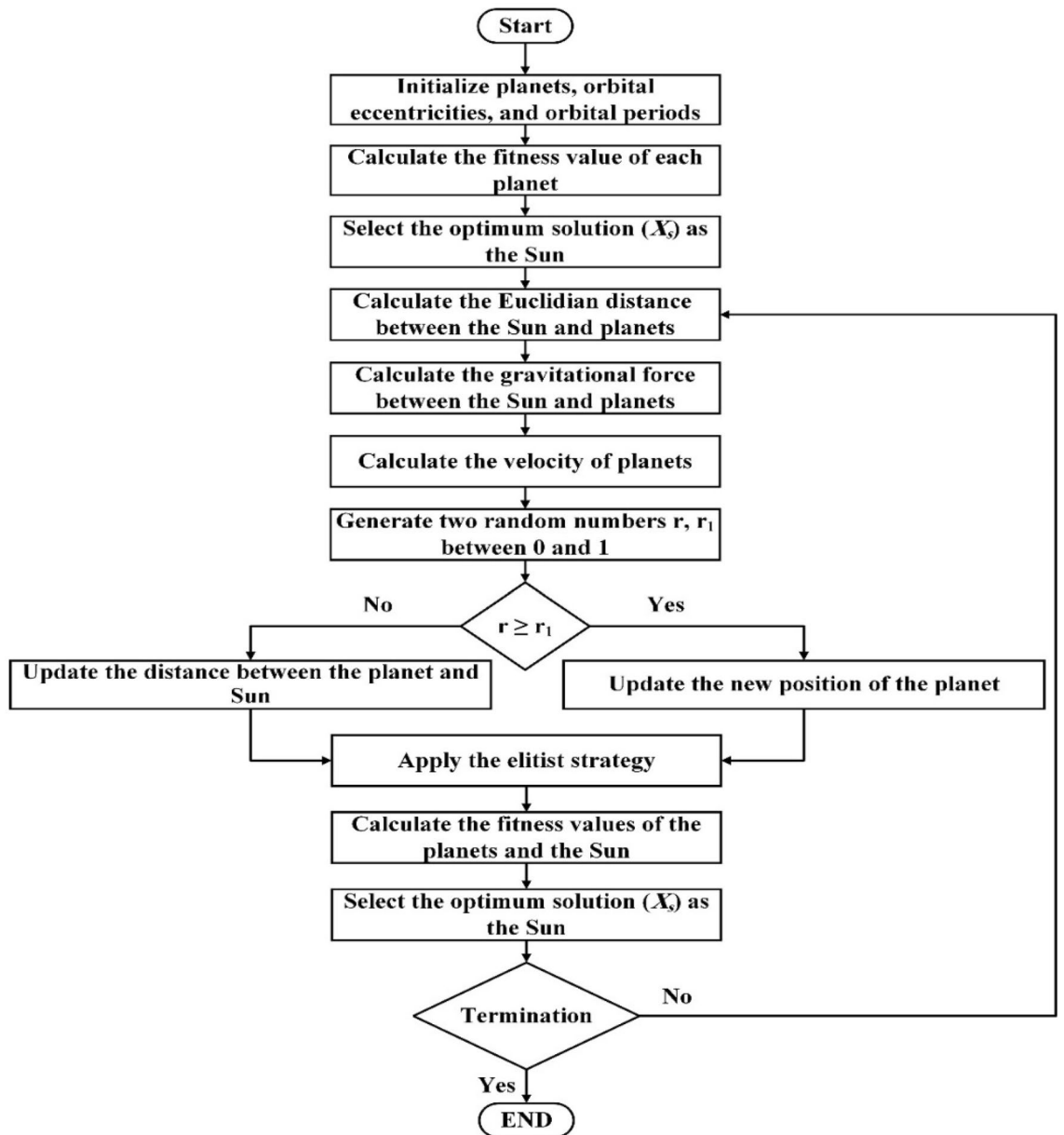
Figure 2. The flowchart of the KOA algorithm.

$$X_i^j = rand_{[0,1]} \times \left(X_{i,up}^j - X_{i,low}^j \right) + X_{i,low}^j \tag{30}$$

where X_i^j represents the ith planet of jth decision variable in the search space. $X_{i,up}^j$ and $X_{i,low}^j$ denote the maximum and minimum bounds, respectively.

The orbital ith planet eccentricity (e_i) is initialized using Eq. (31):

$$e_i = rand_{[0,1]} \tag{31}$$

The orbital ith planet period (T_i) is initialized using Eq. (32):

$$T_i = |r| \tag{32}$$

where r is a random number produced using the normal distribution.

Defining the Euclidian distance
The Euclidian distance ($R_i(t)$) between the Sun $X_{s,j}^t$ and a planet $X_{i,j}^t$ is defined as:

$$R_i(t) = \sqrt{\sum_{j=1}^{d} \left(X_{s,j}^t - X_{i,j}^t \right)^2} \tag{33}$$

where d stands for the problem dimension.

Defining the gravitational force
The gravitational force ($F_{g_i}(t)$) can be calculated using Eq. (34):

$$F_{g_i}(t) = e_i \times \mu(t) \times \frac{\overline{M_s} \times \overline{m_i}}{\overline{R_i}^2 + \varepsilon} + r_1 \tag{34}$$

where $\overline{M_s}$ and $\overline{m_i}$ refer to the normalized mass quantities of the Sun and planet, respectively. ε is a small number. μ is the constant of universal gravity. r_1 is a random number ranging from 0.0 to 1.0. $\overline{R_i}$ is the normalized value of R_i.

Calculating planets' velocity
The planet's orbital speed V_i^t as it orbits the Sun is defined as:

$$V_i^t = \begin{cases} l \times (2r_4 X_i - X_b) + \ddot{\mathfrak{l}} \times (X_a - X_b) + \left(1 - \overline{R_i}\right) \\ \times \xi \times U_1 \times r_5 \times \left(X_{i,up} - X_{i,low}\right), \overline{R_i} \leq 0.5 \\ r_4 \times L \times (X_a - X_i) + \left(1 - \overline{R_i}\right) \\ \times \xi \times U_2 \times r_5 \times \left(r_3 X_{i,up} - X_{i,low}\right), Otherwise \end{cases} \tag{35}$$

where r_3, r_4, and r_5 are random numbers ranging from 0.0 to 1.0. X_a and X_b depict randomly chosen solutions from the population. ξ serves as an indicator to reorient the search.

Updating planets' positions
The new position of each planet is updated using Eq. (36):

$$X_i^{t+1} = X_i^t + \xi \times V_i^t + \left(F_{g_i}^t + |r| \right) \times U \times \left(X_s^t - X_i^t \right) \tag{36}$$

Updating the distance between the planets and the Sun
The Sun's distance from each planet is updated using Eq. (37):

$$X_i^{t+1} = X_i^t \times U_1 + (1 - U_1) \times \left(\frac{X_i^t + X_s + X_a^t}{3} + h \times \left(\frac{X_i^t + X_s + X_a^t}{3} - X_b^t \right) \right) \tag{37}$$

where h is a variable used to regulate how far the Sun is from the planet i.

Elitism
The elitist strategy is described as

$$X_{i,new}^{t+1} = \begin{cases} X_i^{t+1}, f\left(X_i^{t+1}\right) \leq f\left(X_i^t\right) \\ X_i^t, \quad Otherwise \end{cases} \tag{38}$$

Nutcracker optimization algorithm (NOA)
NOA models its behavior after Clark's nutcrackers, delineated by two distinct techniques: the foraging and storage technique and the cache-search and recovery technique[41]. The algorithm's operational processes are graphically outlined in the accompanying flow chart, depicted in Fig. 3. This flow chart offers a visual representation of the sequential steps undertaken by the NOA, aligning with the algorithm's emulation of the nutcrackers' natural behaviors.

NOA is summed up in the following steps:

Initialization process
The NOA population is initialized by

$$X_{i,j}^t = \left(U_j - L_j \right) \cdot RM + L_j \tag{39}$$

where $X_{i,j}^t$ indicates the ith nutcracker (feasible solution) of the jth decision variable in generation t. U_j and L_j denote the jth decision variable maximum and minimum bounds, respectively. RM represents a random vector ranging from 0.0 to 1.0.
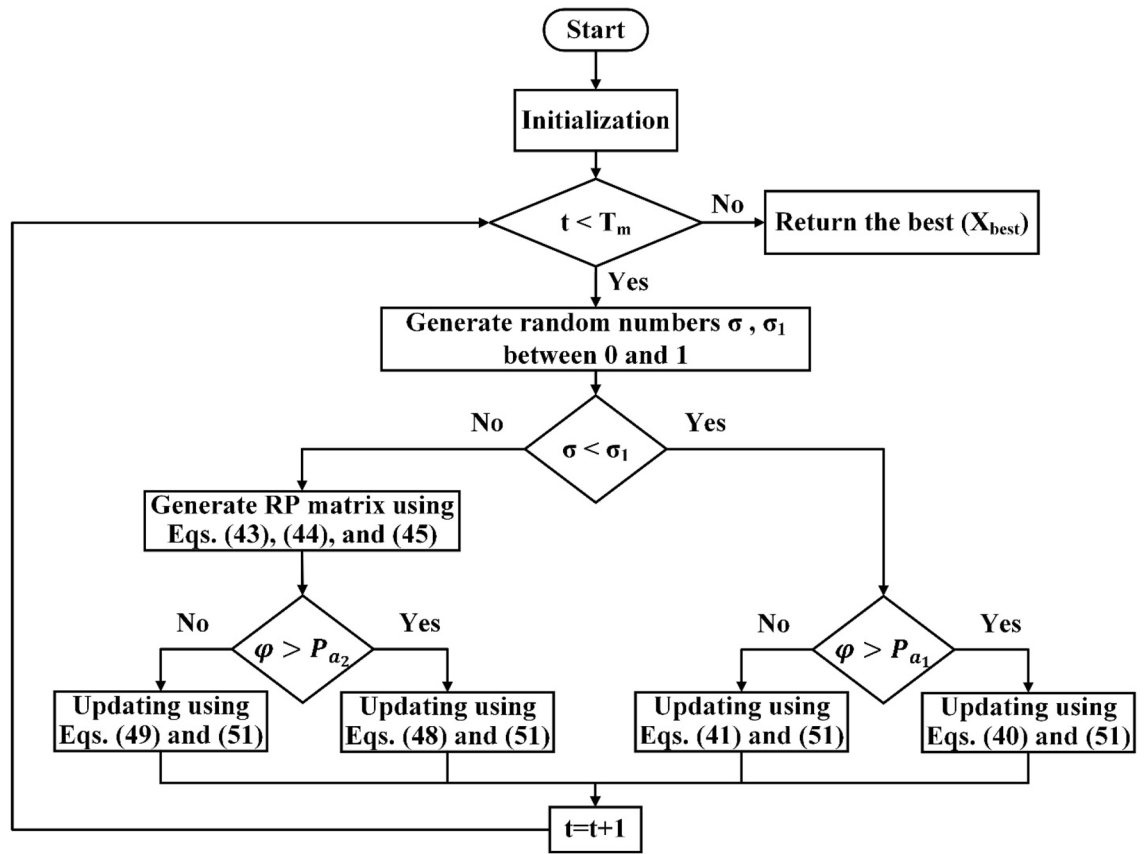
Figure 3. The NOA algorithm flowchart.

Foraging and storage technique
This technique replicates the initial conduct observed in nutcrackers, manifesting during the summer and autumn seasons to gather pine seeds and hoard them. As a result, this technique can be bifurcated into two principal stages: foraging and storage. These stages are expounded upon below:

<u>Foraging stage.</u>   Every nutcracker starts by examining the cone containing the seeds, as shown in Eq. (40).

$$X_i^{t+1} = \begin{cases} X_{i,j}^t, & \tau_1 < \tau_2 \\ \begin{cases} X_{m,j}^t + \gamma \cdot \left(X_{A,j}^t - X_{B,j}^t \right) + \mu \cdot \left(r^2 \cdot U_j - L_j \right), & t \le T_m/2 \\ X_{C,j}^t + \mu \cdot \left(X_{A,j}^t - X_{B,j}^t \right) + \mu \cdot \left(r_1 < \delta \right) \cdot \left(r^2 \cdot U_j - L_j \right), & Otherwise \end{cases}, & Otherwise \end{cases} \quad (40)$$

where γ is a randomly produced number based on the levy flight. A, B, and C are three indicators chosen at random from the population. τ_1, τ_2, r, and r_1 are random numbers ranging from 0.0 to 1.0. $X_{m,j}^t$ is the average of all solutions in iteration t. μ is a number produced using random numbers ranging from 0 to 1, levy-flight, and normal distribution. δ is the likelihood of nutcrackers travelling across the entire search space to look for unreachable locations.

<u>Storage stage.</u>   Nutcrackers start by moving the food acquired in the earlier stage to temporary storage facilities, which can be expressed as follows:

$$X_i^{t+1(new)} = \begin{cases} X_i^t + \mu \cdot \left(X_{best}^t - X_i^t \right) \cdot |\lambda| + r_1 \cdot \left(X_A^t - X_B^t \right), & \tau_1 < \tau_2 \\ X_{best}^t + \mu \cdot \left(X_A^t - X_B^t \right), & \tau_1 < \tau_3 \\ X_{best}^t \cdot l, & Otherwise \end{cases} \quad (41)$$

where $X_i^{t+1(new)}$ denotes a new location in the nutcrackers' storage region in iteration t. X_{best}^t indicates the best solution obtained even now. λ is a number produced based on levy flight. l is a linearly decreasing factor from 1.0 to 0.0.
The interchange between the foraging and storage stages is adopted using Eq. (42):

$$X_i^{t+1} = \begin{cases} Eq.(40), \ \varphi > P_{a_1} \\ Eq.(41), \ Otherwise \end{cases} \tag{42}$$

where φ refers to a random number ranging from 0.0 to 1.0, and P_{a_1} represents a linearly decreasing probability value from 1.0 to 0.0.

Cache-search and recovery technique
This technique simulates the second behavior of nutcrackers, which involves looking for and retrieving storage spaces during winter and spring. Therefore, this technique can be bifurcated into two principal stages: cache search and recovery. These stages are expounded upon below:

Cache-search stage.　The nutcrackers start to identify their caches using a spatial memory methodology. For simplicity, NOA supposes that there are just two Reference Points (*RPs*) (objects) per cache. as shown in Eq. (43).

$$RPs = \begin{bmatrix} RP_{1,1}^t & RP_{1,2}^t \\ \vdots & \vdots \\ RP_{i,1}^t & RP_{i,2}^t \\ \vdots & \vdots \\ RP_{N,1}^t & RP_{N,2}^t \\ \vdots & \vdots \end{bmatrix} \tag{43}$$

where $RP_{i,1}^t$ and $RP_{i,2}^t$ represent *RPs* of ith nutcracker cache position in generation t.
The $RP_{i,1}^t$ and $RP_{i,2}^t$ are described as follows:

$$RP_{i,1}^t = \begin{cases} X_i^t + \alpha \cdot \cos(\theta) \cdot \left(X_A^t - X_B^t\right) + \alpha \cdot RP, \ \theta = \pi/2 \\ X_i^t + \alpha \cdot \cos(\theta) \cdot \left(X_A^t - X_B^t\right), \quad\quad\quad\quad Otherwise \end{cases} \tag{44}$$

$$RP_{i,2}^t = \begin{cases} X_i^t + (\alpha \cdot \cos(\theta) \cdot ((U - L) \cdot \tau_3 + L) + \alpha \cdot RP) \cdot U_2, \ \theta = \pi/2 \\ X_i^t + \alpha \cdot \cos(\theta) \cdot ((U - L) \cdot \tau_3 + L) \cdot U_2, \quad\quad\quad\quad Otherwise \end{cases} \tag{45}$$

where α linearly decreases from one to zero. X_A^t is the Ath nutcracker cache position in iteration t. θ stands for the nutcracker angle of view, which is randomly selected between 0 and π. *RP* is a random position.
Nutcracker's new position can be updated via $RP_{i,1}^t$:

$$X_i^{t+1} = \begin{cases} X_i^t, \quad f\left(X_i^t\right) < f\left(RP_{i,1}^t\right) \\ RP_{i,1}^t, \ Otherwise \end{cases} \tag{46}$$

If the nutcracker is unable to recall where he buried his food utilizing $RP_{i,1}^t$, $RP_{i,2}^t$ will be used. Therefore, $RP_{i,2}^t$ is used to update Nutcracker spatial memory via Eq. (47):

$$X_i^{t+1} = \begin{cases} X_i^t, \quad f\left(X_i^t\right) < f\left(RP_{i,2}^t\right) \\ RP_{i,2}^t, \ Otherwise \end{cases} \tag{47}$$

The exchange between $RP_{i,1}^t$ and $RP_{i,2}^t$ is achieved as follows:

$$X_i^{t+1} = \begin{cases} Eq.(46), \ f\left(Eq.(46)\right) < f\left(Eq.(47)\right) \\ Eq.(47), \ Otherwise \end{cases} \tag{48}$$

Recovery stage.　When the nutcracker can recall the cache location using either $RP_{i,1}^t$ or $RP_{i,2}^t$, there are two outcomes for each: either there is food or there isn't. This process can be expressed as follows:

$$X_i^{t+1} = \begin{cases} \begin{cases} X_{i,j}^t, & \tau_3 < \tau_4 \\ X_{i,j}^t + r_1 \cdot \left(X_{best,j}^t - X_{i,j}^t\right) + r_2 \cdot \left(RP_{i,1}^t - X_{C,j}^t\right), & Otherwise \end{cases}, \ \tau_7 < \tau_8 \\ \begin{cases} X_{i,j}^t, & \tau_5 < \tau_6 \\ X_{i,j}^t + r_1 \cdot \left(X_{best,j}^t - X_{i,j}^t\right) + r_2 \cdot \left(RP_{i,2}^t - X_{C,j}^t\right), & Otherwise \end{cases}, \ Otherwise \end{cases} \tag{49}$$

where $\tau_3, \tau_4, \tau_5, \tau_6, \tau_7$, and τ_8 are random numbers ranging from 0.0 to 1.0.
The interchange between the cache-search and recovery stages is adopted using Eq. (50):

$$X_i^{t+1} = \begin{cases} Eq.(48), \ \varphi > P_{a_2} \\ Eq.(49), \ Otherwise \end{cases} \tag{50}$$

where P_{a_2} corresponds to a probability value of 0.2.
Nutcracker's current position can be enhanced as follows:

$$X_i^{t+1} = \begin{cases} X_i^{t+1}, f\left(X_i^{t+1}\right) < f\left(X_i^t\right) \\ X_i^t, \quad Otherwise \end{cases} \tag{51}$$

Dandelion algorithm

The Dandelion Algorithm (DA) emulates the prolonged aerial voyage of dandelion seeds, a journey characterized by three distinct phases: ascent, descent, and settlement[42]. The computational procedures of the algorithm are graphically depicted in the accompanying flowchart, Fig. 4, serving as an illustrative overview of the DA's operational process.

DA is summed up in the following steps.

Initialization and configuration of algorithm parameters
The initial population of dandelion seeds is generated using the following equation:

$$X_i = rand \times (UB - LB) + LB \tag{52}$$

where X_i indicates the ith dandelion seed (feasible solution). *rand* represents a random value between [0, 1]. *LB* and *UB* represent the decision variables' maximum and minimum bounds, respectively.

Ascending phase
Dandelion seeds disperse from their parent plant once they attain a suitable height. This stage comprises two potential scenarios for the movement of dandelion seeds, which are contingent on factors such as wind speed, air resistance, and humidity.
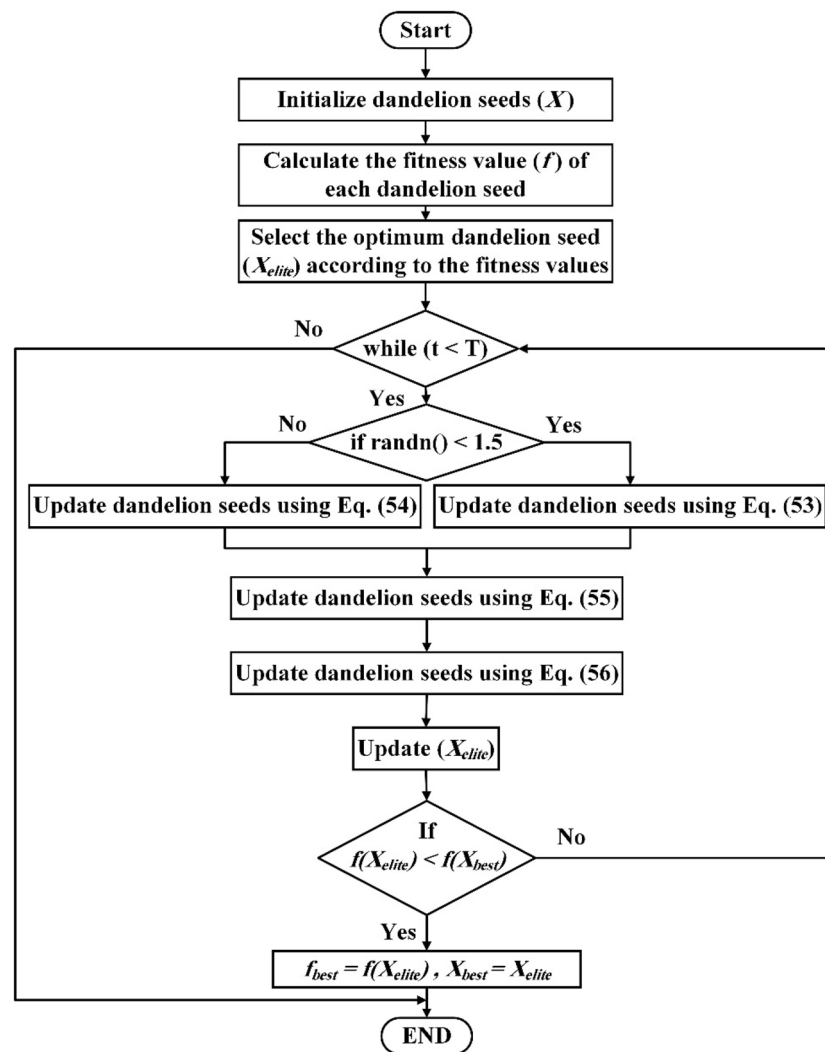
Figure 4. The suggested DA algorithm flowchart.

<u>Case 1.</u> With increasing wind strength, the dandelion achieves greater height and scatters its seeds over a wider range. This scenario can be mathematically represented as follows:

$$X_{t+1} = X_t + rand * \left(\frac{t^2}{T^2} - \frac{2t}{T} + 1 \right) * \frac{1}{e^{2\theta}} * \frac{sin(2\theta)}{2} * lnY * (X_s - X_t) \tag{53}$$

where X_t represents the position of the seed at iteration t. X_{t+1} denotes the seed position at iteration $t+1$. X_s signifies a random location within the search space. The term lnY represents the logarithmic normal distribution. θ represents a random number falling within the range of $[-\pi, \pi]$. T represents the maximum number of iterations.

<u>Case 2.</u> Under rainy conditions, dandelion seeds encounter challenges in achieving optimal ascent against the wind. This situation can be expressed mathematically as follows:

$$X_{t+1} = X_t * \left(1 - rand * \left(\frac{T^2 - 2T + t^2 - 2t + 2}{T^2 - 2T + 1} \right) \right) \tag{54}$$

Descent phase
This phase promotes the exploration process and can be mathematically represented as follows:

$$X_{t+1} = X_t - rand * \left(\frac{t^2}{T^2} - \frac{2t}{T} + 1 \right) * \beta_t * \left(\left(\frac{1}{pop} \sum_{i=1}^{pop} X_i \right) - rand * \left(\frac{t^2}{T^2} - \frac{2t}{T} + 1 \right) * \beta_t * X_t \right) \tag{55}$$

where β_t represents Brownian motion and is a random number drawn from a normal distribution. *pop* is the population size.

Landing phase
The landing phase facilitates the exploitation process and can be defined by the following equation:

$$X_{t+1} = X_{elite} + \frac{s * w * \Gamma(1+\beta) * sin\left(\frac{\pi\beta}{2}\right)}{|t|^{\frac{1}{\beta}} * \Gamma\left(\frac{1+\beta}{2}\right) * \beta * 2^{\left(\frac{\beta-1}{2}\right)}} * rand * \left(\frac{t^2}{T^2} - \frac{2t}{T} + 1 \right) * \left(X_{elite} - \frac{2t}{T} * X_t \right) \tag{56}$$

where X_{elite} indicates the seed's optimal position during *i*th iteration. *s* set at a fixed value of 0.01. *w* and *t* are random numbers within the range of $[0, 1]$. β is fixed at 1.5.

Termination
The DA algorithm concludes its execution and provides the optimal solution vector after a certain number of iterations (T).

Results and discussion
The microgrid model proposed in this study is situated in the city of Benban, located within the Aswan Governorate. Geographically, Benban is positioned at a longitude of 32.870°E and a latitude of 24.440°N. Figure 5 displays the consistent fluctuation of wind speed throughout this period, reaching its peak value of 12.4470 m/s at 6 p.m.[43]. This value then gradually diminishes to reach zero by 5 p.m., remaining at this level until 6 a.m. the
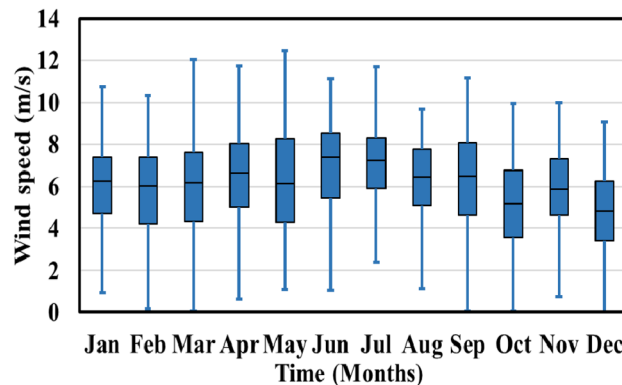

Figure 5. Monthly wind speed.

following day[44]. In contrast, Fig. 6 illustrates a gradual and nonlinear rise in solar irradiance throughout the day, starting from zero at 6 a.m. and peaking at noon with a maximum recorded value of 1187.59 W/m^2.

The associated costs for electricity transactions in this microgrid scenario are as follows: purchasing electricity from the utility grid costs 0.20 \$/kWh from midnight to 8 a.m., 0.50 \$/kWh from 8 a.m. to 4 p.m., and 0.30 \$/kWh from 4 p.m. to midnight, while selling electricity back to the utility is priced at 0.06685 \$/kWh[45]. Additionally, Fig. 7 displays the monthly distribution of load demand throughout the year, indicating a peak demand of 2115.40 kW at 5:00 p.m. and a minimum demand of 290.0 kW at 10:00 a.m.[46]. The initial price of electricity remains constant at 0.5 \$/kWh within each respective period.

To evaluate the effectiveness of the proposed optimization technique, a comparative analysis of performance is conducted. Four distinct operational scenarios (each corresponding to different optimization techniques) are explored for the microgrid model incorporating RGDP DR. This investigation aims to elucidate the impact of the recommended optimization strategy.

Across all scenarios, crucial metrics including energy consumption, decrease in energy consumption, incentives, and penalties result in values of 707,959 kWh, zero, zero, and zero, respectively. The pricing framework encompasses maximum and minimum boundaries set at 0.550 and 0.450 \$/kWh, respectively. Figure 8 illustrates the transformation in economic load demand profiles, both before and after the implementation of RGDP DR. Furthermore, the alteration in electricity pricing resulting from RGDP DR is visually presented in Fig. 9, calculated using Eq. (28). The results of implementing optimization techniques for obtaining the optimal size of RES for the microgrid will be discussed in the following subsections.

Scenario 1: DA algorithm

The proposed microgrid configuration entails capacities for PV, wind, battery, and converter set at 6579 kW, 937 kW, 3482 kW, and 3212 kW, respectively. These designations align with the life cycle emissions of 2,696,972 kgCO$_2$-eq/Year, the total microgrid cost of 1,246,864 \$/Year, and the customer bill totaling 3,845,911 \$/Year, as elucidated within Table 2. The hourly output power from each Renewable Energy Source (RES) throughout 24 h is visually illustrated in Fig. 10, employing the Dandelion Algorithm (DA).

Scenario 2: PSO algorithm

The capacities of PV, wind, battery, and converter are 6566 kW, 926 kW, 3523 kW, and 3211 kW, respectively. The life cycle emissions amount to 2,694,292 kgCO$_2$-eq/Year, the total microgrid cost is 1,246,866 \$/Year, and
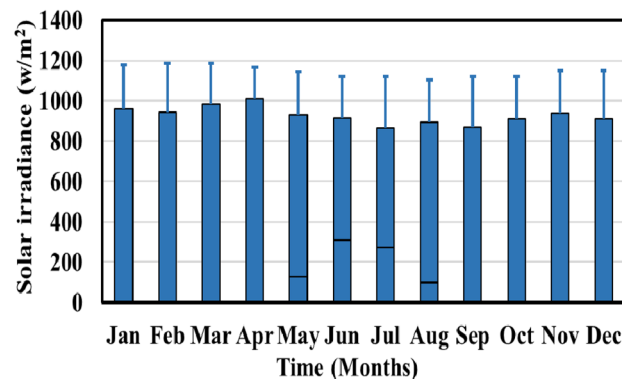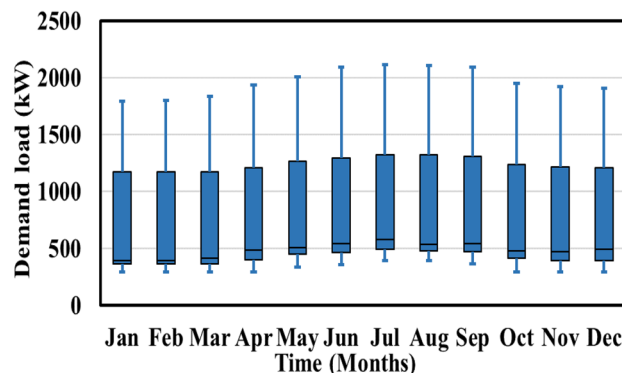

Figure 6. Monthly solar irradiance.
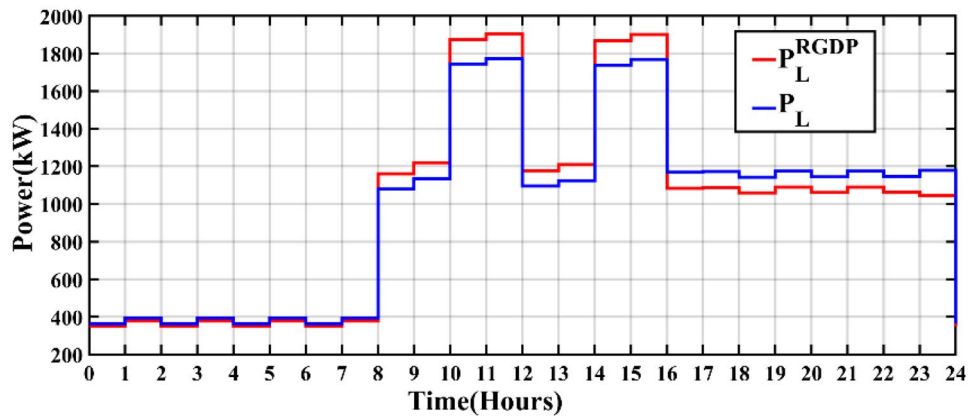

Figure 7. Monthly demand profile.

Figure 8. RGDP DR demand profile.
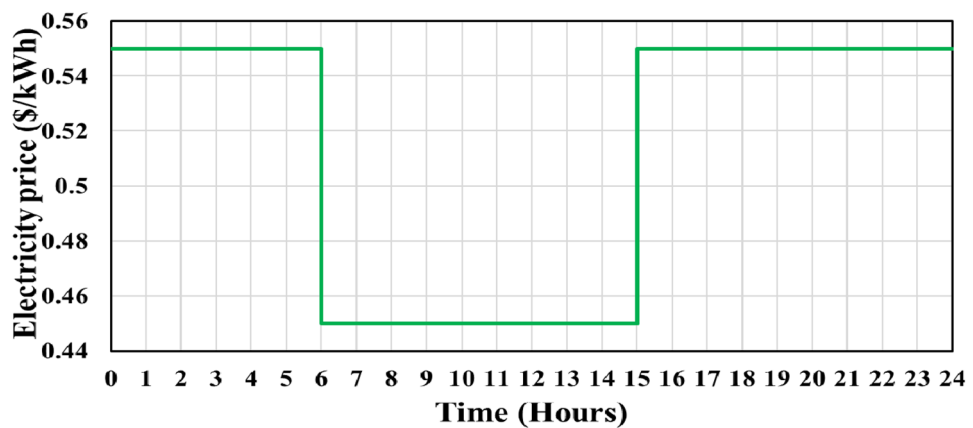
Figure 9. The generated electricity cost with RGDP DR deployment.

	DA	PSO	NOA	KOA
PV capacity (kW)	6579	6566	6542	6551
Wind capacity (kW)	937	926	924	908
Battery capacity (kW)	3482	3523	3537	3617
Converter capacity (kW)	3212	3211	3192	3241
Life cycle emissions (LCE) (kgCO$_2$-eq/yr)	2,696,972	2,694,292	2,690,314	2,683,489
Emission cost ($/year)	53,940	53,886	53,807	53,670
Components cost ($/year)	1,192,924	1,192,980	1,193,064	1,193,235
Total cost of microgrid ($/year)	1,246,864	1,246,866	1,246,871	1,246,905
Customer bill ($/year)	3,845,911	3,846,043	3,846,108	3,846,235

Table 2. Overall comparison of the studied scenarios.

the customer bill reaches 3,846,043 $/Year, as detailed in Table 2. The output power of each RES for each hour over a single day is depicted in Fig. 11 through the application of PSO.

Scenario 3: NOA algorithm

The capacities of PV, wind, battery, and converter are 6542 kW, 924 kW, 3537 kW, and 3192 kW, respectively. The life cycle emissions amount to 2,690,314 kgCO$_2$-eq/Year, the total microgrid cost is 1,246,871 $/Year, and the customer bill reaches 3,846,108 $/Year, as detailed in Table 2. The output power of each RES for each hour over a single day is illustrated in Fig. 12, utilizing the NOA.
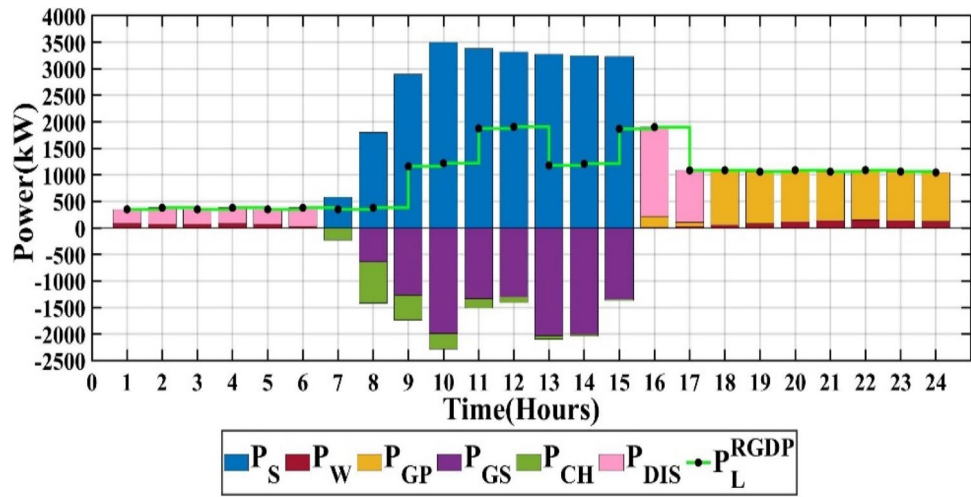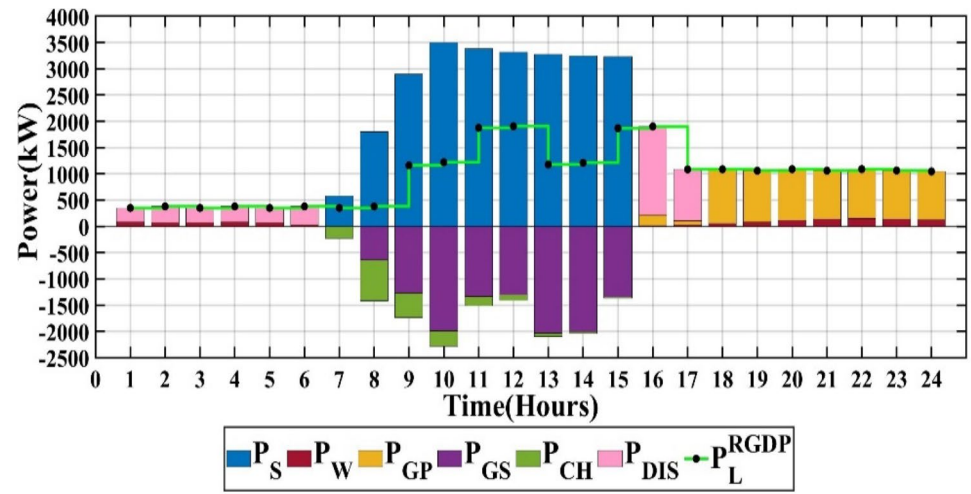
Figure 10. Scenario 1 of MG.
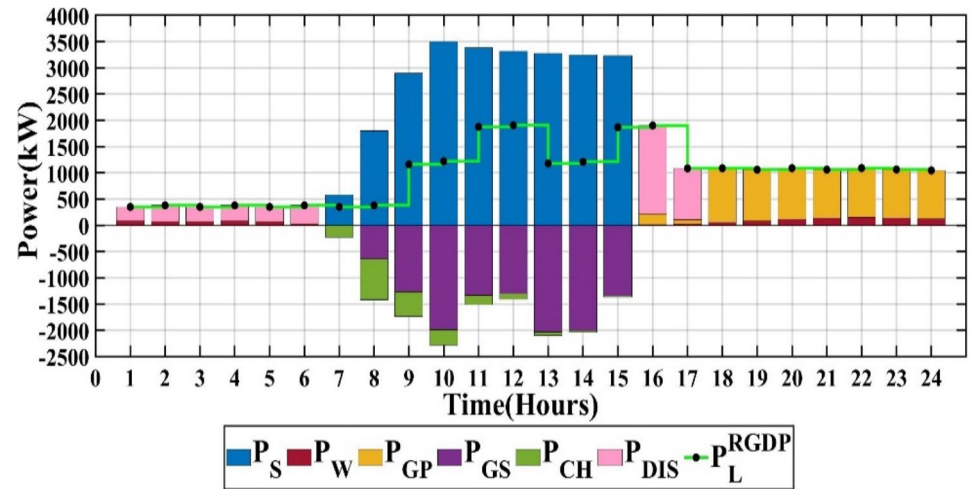

Figure 11. Scenario 2 of MG.
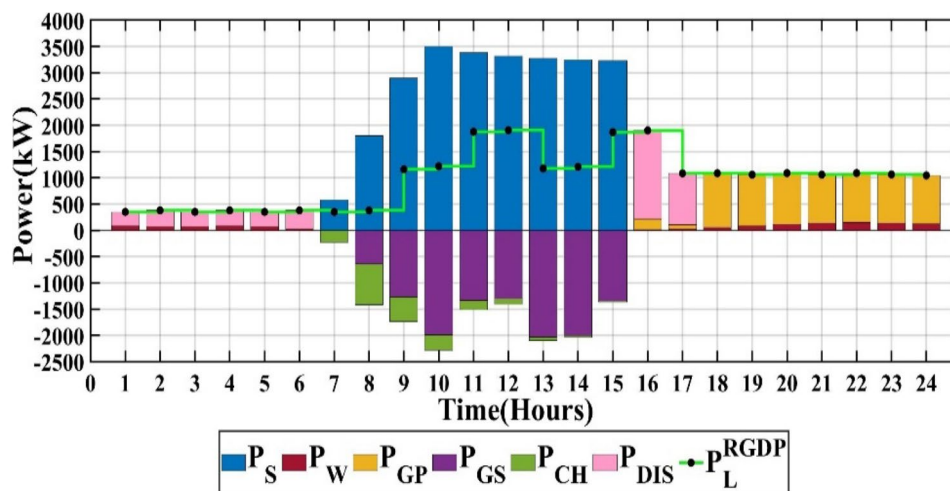

Figure 12. Scenario 3 of MG.

Figure 13. Scenario 4 of MG.

Scenario 4: KOA algorithm

The capacities of PV, wind, battery, and converter are 6551 kW, 908 kW, 3617 kW, and 3241 kW, respectively. The life cycle emissions amount to 2,683,489 kgCO$_2$-eq/Year, the total microgrid cost is 1,246,905 \$/Year, and the customer bill reaches 3,846,235 \$/Year, as detailed in Table 2. The output power of each Renewable Energy Source (RES) for each hour over a single day is depicted in Fig. 13 using the KOA.

Conclusion

This paper introduces an innovative methodology for determining the optimal size of a grid-connected microgrid (MG) through an energy management framework with two primary objectives: minimizing the total annual cost and reducing life cycle emissions. The devised microgrid architecture incorporates distributed energy resources such as Battery Energy Storage Systems (BESS), wind turbines (WT), and photovoltaics (PV). A comprehensive mathematical model is presented, integrating the RGDP-DR approach to ascertain the optimal grid-connected MG size. The RGDP DR strategy is devised to address the disparities between demand load and renewable energy source (RES) generation.

The study conducts a thorough comparative analysis involving four optimization techniques: Dandelion Algorithm (DA), Particle Swarm Optimization (PSO), Nature-Inspired Optimization Algorithm (NOA), and Knowledge Optimization Algorithm (KOA). The evaluation metrics encompass life cycle emissions, the optimal microgrid cost, and customer billing. Simulation results demonstrate the superiority of the proposed DA in achieving the lowest microgrid cost and customer bill, outperforming the other optimization methods. Importantly, this evaluation considers only 10% of the load in the management strategy.

DA demonstrates a minimal total annual cost of \$1,246,864, leading to a marginal difference compared to other techniques. PSO closely follows, with a total annual cost of \$1,246,866, showing comparable performance to DA. NOA and KOA yield similar results, with total annual costs of \$1,246,871 and \$1,246,905, respectively. In terms of the annual customer bill, DA results in the lowest at \$3,845,911, showcasing a distinct advantage over other optimization methods. PSO closely trails DA, with an annual customer bill of \$3,846,043, indicating competitive performance. NOA and KOA exhibit comparable annual customer bills, standing at \$3,846,108 and \$3,846,235, respectively.

In conclusion, this research establishes that the proposed framework offers an optimal approach for developing a sustainable microgrid driven by renewable energy sources. The numerical evidence supports the claim of the Dandelion Algorithm's effectiveness, particularly in minimizing both microgrid cost and customer billing, even when considering only 10% of the load in the management strategy.

In future research, the proposed RGDP-based DR may be employed on interconnected multi-nano grids and microgrids to find the optimal configuration and size of these interconnected microgrids, considering MG configurations, load types, and uncertainties.

Data availability

The datasets generated during the current study are available from the corresponding author upon reasonable request.

References

1. Salah, S. I., Eltaweel, M. & Abeykoon, C. Towards a sustainable energy future for Egypt: A systematic review of renewable energy sources, technologies, challenges, and recommendations. *Clean. Eng. Technol.* **8**, 100497 (2022).
2. Albalawi, H., Eisa, A. & El Aggoune, H. Bankruptcy problem in energy warehouse: Applications and challenges. *Ain Shams Eng. J.* **1**, 102011 (2022).
3. Jasim, A. M., Jasim, B. H., Neagu, B. C. & Alhasnawi, B. N. Efficient optimization algorithm-based demand-side management program for smart grid residential load. *Axioms* **12**, 33 (2023).
4. Aybar-Mejía, M., Villanueva, J., Mariano-Hernández, D., Santos, F. & Molina-García, A. A review of low-voltage renewable micro-grids: Generation forecasting and demand-side management strategies. *Electronics* **10**, 2093 (2021).
5. Qiu, D. *et al.* Strategic retail pricing and demand bidding of retailers in electricity market: A data-driven chance-constrained programming. *Adv. Appl. Energy* **7**, 100100 (2022).
6. Battula, A. R., Vuddanti, S. & Salkuti, S. R. A day ahead demand schedule strategy for optimal operation of microgrid with uncertainty. *Smart Cities* **6**, 491–509 (2023).
7. Ribó-Pérez, D., Larrosa-López, L., Pecondón-Tricas, D. & Alcázar-Ortega, M. A critical review of demand response products as resource for ancillary services: International experience and policy recommendations. *Energies* **14**, 846 (2021).
8. Chreim, B., Esseghir, M. & Merghem-Boulahia, L. Recent sizing, placement, and management techniques for individual and shared battery energy storage systems in residential areas: A review. *Energy Rep.* **11**, 250–260 (2024).
9. Elazab, R., Abdelnaby, A. T. & Ali, A. A. Impacts of multiple demand-side management strategies on microgrids planning: A literature survey. *Clean Energy* **8**, 36–54 (2024).
10. Moradi-Sarvestani, S., Jooshaki, M., Fotuhi-Firuzabad, M. & Lehtonen, M. Incorporating direct load control demand response into active distribution system planning. *Appl. Energy* **339**, 120897 (2023).
11. Enrich, J., Li, R., Mizrahi, A. & Reguant, M. Measuring the impact of time-of-use pricing on electricity consumption: Evidence from Spain. *J. Environ. Econ. Manage* **123**, 102901 (2024).
12. Oskouei, M. Z. *et al.* A critical review on the impacts of energy storage systems and demand-side management strategies in the economic operation of renewable-based distribution network. *Sustainability* **14**, 2110 (2022).
13. Kanakadhurga, D. & Prabaharan, N. Demand side management in microgrid: A critical review of key issues and recent trends. *Renew. Sustain. Energy Rev.* **156**, 111915 (2022).
14. Elio, J., Phelan, P., Villalobos, R. & Milcarek, R. J. A review of energy storage technologies for demand-side management in industrial facilities. *J. Clean. Prod.* **307**, 127322 (2021).
15. Phani Raghav, L., Seshu Kumar, R., Koteswara Raju, D. & Singh, A. R. Analytic hierarchy process (AHP): Swarm intelligence based flexible demand response management of grid-connected microgrid. *Appl. Energy* **306**, 118058 (2022).
16. Seshu Kumar, R., Phani Raghav, L., Koteswara Raju, D. & Singh, A. R. Impact of multiple demand side management programs on the optimal operation of grid-connected microgrids. *Appl. Energy* **301**, 117466 (2021).
17. Mohammadjafari, M., Ebrahimi, R. & Parvin Darabad, V. Optimal energy management of a microgrid incorporating a novel efficient demand response and battery storage system. *J. Electr. Eng. Technol.* **15**, 571–590 (2020).
18. Hajiamoosha, P., Rastgou, A., Bahramara, S. & Bagher Sadati, S. M. Stochastic energy management in a renewable energy-based microgrid considering demand response program. *Int. J. Electr. Power Energy Syst.* **129**, 106791 (2021).
19. Mulleriyawage, U. G. K. & Shen, W. X. Impact of demand side management on optimal sizing of residential battery energy storage system. *Renew. Energy* **172**, 1250–1266 (2021).
20. Kumar, M. & Tyagi, B. Optimal energy management and sizing of a community smart microgrid using demand side management with load uncertainty. *ECTI Trans. Comput. Inf. Technol.* **15**, 186–197 (2021).
21. Kumar, R. S., Raghav, L. P., Raju, D. K. & Singh, A. R. Customer-oriented energy demand management of grid connected microgrids. *Int. J. Energy Res.* **45**, 18695–18712 (2021).
22. Astriani, Y., Shafiullah, G. M. & Shahnia, F. Incentive determination of a demand response program for microgrids. *Appl. Energy* **292**, 116624 (2021).
23. Hakimi, S. M., Hasankhani, A., Shafie-khah, M., Lotfi, M. & Catalão, J. P. S. Optimal sizing of renewable energy systems in a microgrid considering electricity market interaction and reliability analysis. *Electr. Power Syst. Res.* **203**, 107678 (2022).
24. Yu, Z. X., Li, M. S., Xu, Y. P., Aslam, S. & Li, Y. K. Techno-economic planning and operation of the microgrid considering real-time pricing demand response program. *Energies* **14**, 4597 (2021).
25. Das, S. & Barik, A. K. Opposition-based competitive swarm optimizer for optimal sizing and siting of DG units in radial system. *Lect. Not. Electr. Eng.* **823**, 269–282 (2022).
26. Jadoun, V. K. *et al.* Optimal scheduling of dynamic pricing based V2G and G2V operation in microgrid using improved elephant herding optimization. *Sustainability* **13**, 7551 (2021).
27. Duan, H., Li, Q., Li, Y., Zhang, J. & Xie, Y. *Comparative Study of Microgrid Optimal Scheduling Under Multi-optimization Algorithm Fusion* (Springer, 2023).
28. Balasubramanyam, P. & Sood, V. K. Dynamic energy management system of microgrid using AI techniques: A comprehensive & comparative study. *DC Microgrids* **1**, 101–120 (2021).
29. Kiptoo, M. K. *et al.* Integrated approach for optimal techno-economic planning for high renewable energy-based isolated microgrid considering cost of energy storage and demand response strategies. *Energy Convers. Manag.* **215**, 112917 (2020).
30. Gamil, M. M. *et al.* Optimal multi-objective sizing of a residential microgrid in Egypt with different ToU demand response percentages. *Sustain. Cities Soc.* **75**, 103293 (2021).
31. Kumar, R. S., Raghav, L. P., Raju, D. K. & Singh, A. R. Intelligent demand side management for optimal energy scheduling of grid connected microgrids. *Appl. Energy* **285**, 116435 (2021).
32. Hassan, A., Al-Abdeli, Y. M., Masek, M. & Bass, O. Optimal sizing and energy scheduling of grid-supplemented solar PV systems with battery storage: Sensitivity of reliability and financial constraints. *Energy* **238**, 121780 (2022).
33. Zaki Diab, A. A., El-Rifaie, A. M., Zaky, M. M. & Tolba, M. A. Optimal sizing of stand-alone microgrids based on recent metaheuristic algorithms. *Mathematics* **10**, 140 (2022).
34. Elazab, R., Abdelnaby, A. T., Keshta, H. E. & Ali, A. A. Optimal techno-economic feasibility analysis of a grid-tied microgrid considering demand response strategy. *Electr. Power Syst. Res.* **224**, 109768 (2023).
35. ZakiDiab, A. A., Sultan, H. M., Mohamed, I. S., KuznetsovOleg, N. & Do, T. D. Application of different optimization algorithms for optimal sizing of pv/wind/diesel/battery storage stand-alone hybrid microgrid. *IEEE Access* **7**, 119223–119245 (2019).
36. Paliwal, P., Patidar, N. P. & Nema, R. K. Determination of reliability constrained optimal resource mix for an autonomous hybrid power system using particle swarm optimization. *Renew. Energy* **63**, 194–204 (2014).
37. Kumari, J., Subathra, P., Edwin Moses, J. & Shruthi, D. Economic analysis of hybrid energy system for rural electrification using homer. in *Proceedings of IEEE International Conference on Innovations in Electrical, Electronics, Instrumentation and Media Technology, ICIEEIMT 2017*, 151–156 (2017).
38. Bakhshaei, P., Askarzadeh, A. & Arababadi, R. Operation optimization of a grid-connected photovoltaic/pumped hydro storage considering demand response program by an improved crow search algorithm. *J. Energy Storage* **44**, 103326 (2021).
39. Eberhart, R. & Kennedy, J. New optimizer using particle swarm theory. in *Proceedings of the International Symposium on Micro Machine and Human Science*, 39–43 (1995).

40. Abdel-Basset, M., Mohamed, R., Azeem, S. A. A., Jameel, M. & Abouhawwash, M. Kepler optimization algorithm: A new metaheuristic algorithm inspired by Kepler's laws of planetary motion. *Knowl. Based Syst.* **268**, 110454 (2023).
41. Abdel-Basset, M., Mohamed, R., Jameel, M. & Abouhawwash, M. Nutcracker optimizer: A novel nature-inspired metaheuristic algorithm for global optimization and engineering design problems. *Knowl. Based Syst.* **262**, 110248 (2023).
42. Zhao, S., Zhang, T., Ma, S. & Chen, M. Dandelion optimizer: A nature-inspired metaheuristic algorithm for engineering applications. *Eng. Appl. Artif. Intell.* **114**, 105075 (2022).
43. Renewables.ninja. https://www.renewables.ninja/.
44. JRC Photovoltaic Geographical Information System (PVGIS): European Commission. https://re.jrc.ec.europa.eu/pvg_tools/en/.
45. Elazab, R., Saif, O., Amin Metwally, A. M. A. & Daowd, M. New smart home energy management systems based on inclining block-rate pricing scheme. *Clean Energy* **6**, 503–511 (2022).
46. Angizeh, F., Ghofrani, A. & Jafari, M. A. Dataset on hourly load profiles for a set of 24 facilities from industrial, commercial, and residential end-use sectors. *Mendeley Data* (2020).
47. Elazab, R., Abdelnaby, A. T. & Ali, A.A. Impacts of multiple demand-side management strategies on microgrids planning: a literature survey. *Clean Energy* **8**, 36–54 (2024).

Author contributions

Funding

Competing interests

The authors declare no competing interests.

Additional information

Correspondence and requests for materials should be addressed to A.T.A.

Reprints and permissions information is available at www.nature.com/reprints.

Publisher's note Springer Nature remains neutral with regard to jurisdictional claims in published maps and institutional affiliations.